Optics Letters

Adaptive interferometric null testing for unknown freeform optics metrology

Lei Huang,[1,2] Heejoo Choi,[2] Wenchuan Zhao,[2,3] Logan R. Graves,[2] and Dae Wook Kim[2,*]

[1]*Center for Photonics and Electronics, Department of Precision Instruments, Tsinghua University, Beijing 100084, China*
[2]*College of Optical Sciences, University of Arizona, 1630 East University Boulevard, Tucson, Arizona 85721, USA*
[3]*Institute of Optics and Electronics, Chinese Academy of Sciences, Chengdu 610209, China*
*Corresponding author: letter2dwk@hotmail.com

We report an adaptive interferometric null testing method for overcoming the dynamic range limitations of conventional null testing approaches during unknown freeform optics metrology or optics manufacturing processes that require not-yet-completed surface measurements to guide the next fabrication process. In the presented adaptive method, a deformable mirror functions as an adaptable null component for an unknown optical surface. The optimal deformable mirror's shape is determined by the stochastic parallel gradient descent algorithm and controlled by a deflectometry system. An adaptive interferometric null testing setup was constructed, and its metrology data successfully demonstrated superb adaptive capability in measuring an unknown surface. © 2016 Optical Society of America

With the rapid development of freeform optics technology, freeform optical elements have been used to realize a wide range of important applications, including imaging systems, mobile displays, light-emitting diodes, and astronomical/space instruments. Advanced design and fabrication technologies have been developed for producing high-quality freeform optical systems.

During the optics manufacturing process, the in-process (i.e., not-yet-completed) optical surface must be accurately measured in order to guide the iterative fabrication process [1,2]. Although a customized null test [e.g., computer generated holograms (CGHs) or null lens interferometry] can provide high accuracy and precision for known optical surface metrology [3–5], its application is limited to a null or near-null situation. For example, if the test surface is being manufactured, no fixed null configuration is available because the metrology target is an evolving freeform surface. This intrinsic challenge of measuring in-process freeform optics becomes a critical factor in advanced optical fabrication processes.

Other non-null measurement methods, including deflectometry, coordinate measuring machines (CMMs), and profilometers, have been used to measure such in-process optics. However, these methods often have limitations. Due to a delicate calibration process for each configuration, the deflectometry method [6,7] has practical challenges, especially in guiding low-order (e.g., astigmatic surface error) figuring processes. Contact-type approaches such as CMMs or profilometers often require long measurement times, suffer from insufficient spatial resolution, and/or may cause damage to the optical surface.

We report an adaptive interferometric null testing method that overcomes the intrinsic dynamic range limitations of conventional null approaches. In the presented adaptive solution, a deformable mirror (DM) acts as an adaptable null component. The DM's shape is optimized using the stochastic parallel gradient descent (SPGD) algorithm [8]. The updating DM is precisely measured using an *in situ* deflectometry system (DS), which includes a display screen and camera [7,9]. This unique *in situ* adaptive null measurement approach overcomes the limited accuracy/precision issue of a typical DM in the context of adaptive interferometry. The on-demand null condition achieved by the DM and DS enables rapid measurement of unknown freeform surfaces without requiring moving parts (except DM actuators) in the metrology system.

A schematic diagram of the adaptive metrology system including three subsystems (interferometer, DM, and DS) is depicted in Fig. 1. In practice, if the DM's maximum stroke/deformation (e.g., 20 μm) is not sufficient, a nominal static null component such as CGH can be adopted to compensate for the nominal wavefront deformation (e.g., wavefront deformation from the ideal freeform optic). Note that the DM's surface, not its wavefront, is directly measured by the DS in the presented adaptive interferometric null testing. Unlike other common adaptive optics/interferometry applications using a wavefront sensor, such as the Shack–Hartmann sensor for measuring the wavefront at a limited spatial resolution (e.g., 30×30 lenslet array), acquiring a high-resolution DM surface map (e.g., 500×500 pixels) is essential for distinguishing the mid- to high-spatial frequency error of the test optic from the raw data.

When the test optic is inserted into the adaptive metrology system, the initial interference fringes are acquired. Starting from the initial fringe data, the SPGD algorithm works to drive the DM. An online null condition for the unknown freeform
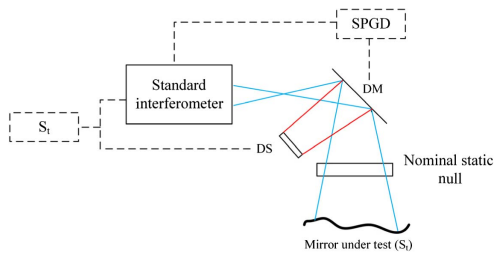
Fig. 1. Schematic adaptive metrology system layout including the standard interferometer, DM, DS, and a nominal static null (optional). Dashed line represents data flow in the processing algorithms. Blue and red lines represent the interferometry and deflectometry beam paths, respectively.
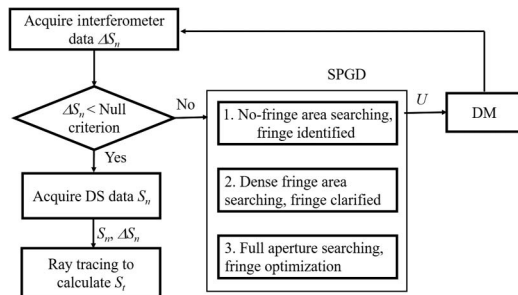
Fig. 2. Schematic data-processing pipeline for adaptive interferometric null testing. Here, U is the control vector for the DM actuators.
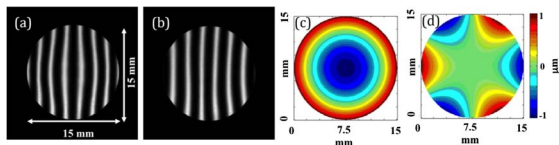
Fig. 3. Raw deflectometry patterns measured by the DS camera. (a) The image pattern is the deformed fringe due to (c) the fourth-order Zernike shape in DM. (b) The pattern is the deformed fringe due to (d) the ninth-order Zernike shape in DM.

surface is created. The overall data-processing pipeline is presented in Fig. 2. The surface shape of the test optic is obtained by combining the results from the *in situ* DS and the interferometer based on Eqs. (1)–(3) as follows:

$$S_t = f(S_n, \Delta S_n), \quad (1)$$

$$\Delta S_n \rightarrow 0, \quad (2)$$

$$S_n = (S_{DS1} - S_{DS0}) + S_{DM0}. \quad (3)$$

Here, S_t is the in-process unknown freeform surface to be measured; S_n is the surface shape of the adaptable null, DM; ΔS_n is the interferometer data measuring the whole metrology system; S_{DS0} is the nominal DM surface shape; S_{DS1} is the final DM surface; and S_{DM0} is the independently calibrated DM's nominal surface shape. Note that Eq. (2) indicates approaching the null condition. Because S_{DM0} is set to be nearly flat, this calibration can be done accurately using a standard interferometer.

As the near-null condition is achieved using the DM, more accurate results are acquired without large retrace errors [10] in the interferometer data. The minimization of the DM data systematic error is achieved by measuring only the change of the DM surface from its nominal shape. Two examples showing raw DS metrology data are presented in Fig. 3 to illustrate the deflectometry patterns for different DM surface shapes.

Some experimental results demonstrating the good DM compensation capability, which show small residual errors after providing large magnitude online nulls, are presented in Table 1. For instance, the residual peak-to-valley (PV) errors are less than ~1.5 µm after creating the ~20 µm PV DM surface change as an adaptable null.

After bulk compensation using DM's large dynamic range, the residual error is measured by the *in situ* DS and compensated in the data-processing pipeline as shown in Fig. 2. Note that the DM surface (compared to the wavefront at a conjugate plane measured by a Shack–Hartmann wavefront sensor) is directly measured with high-spatial resolution (e.g., 500 × 500 pixels across the DM surface) containing all of the mid- to high-spatial frequency surface information, which is critical for guiding the following fabrication process.

An adaptive null algorithm has been developed to control the online DM. The algorithm consists of three major steps utilizing a SPGD-based search, as shown in Fig. 2. The first step is a no-fringe area search and fringe restoration. The second step is a dense fringe detection and relaxation, and the last step is a wavefront decomposition and nulling optimization to satisfy Eq. (2).

To represent a realistic in-process optic in this study, a heavily distorted mirror was prepared by random mechanical pinching to produce a large unknown surface error. An interferometric test could not produce a complete interference fringe

Table 1. Experimental Data Showing DM's Adaptable Nulling Capability for Large Compensation Magnitude in DM Surface Shape Change[a]

Targeting Compensation Magnitude (µm)	Zernike Order No. and Residual Surface Error (µm)				
	Z4	Z5	Z6	Z7	Z8
	(Power)	(Astigmatism)		(Coma)	
PV = 10.061	PV = 0.583 RMS = 0.054	PV = 0.472 RMS = 0.048	PV = 0.454 RMS = 0.051	PV = 0.658 RMS = 0.072	PV = 0.693 RMS = 0.085
PV = 20.122	PV = 1.159 RMS = 0.105	PV = 1.089 RMS = 0.097	PV = 1.078 RMS = 0.102	PV = 1.345 RMS = 0.122	PV = 1.425 RMS = 0.161

[a]This table shows results only up to the eighth Zernike order, which are usually the largest magnitude nulling orders, while the DM used in this study controls up to 52 orthogonal modes.

over the entire optical surface due to its limited dynamic range, as shown in Fig. 4(a).

In the first step, the no-fringe areas such as the upper left and lower right regions in Fig. 4(a) are identified. While monitoring those subregions, a local SPGD algorithm is applied to the DM actuators (more specifically, to the actuator input voltages, U) in each no-fringe area using Eqs. (4)–(6) until the fringes are restored. The judgment value (or figure of merit) J used for guiding the SPGD process in restoring the fringes is defined in Eq. (6)

$$U^{k+1} = U^k + \gamma \delta J \delta U^k, \qquad (4)$$

$$\delta J^k = J(U^k + \delta U^k) - J(U^k), \qquad (5)$$

$$J = \sum_{\text{all}(i,j)} (p_i - p_j)^2. \qquad (6)$$

Here, $U = \{u_m, ..., u_n\}$ is the control signal vector of the actuator voltages; m and n are the index numbers of the actuators; k is the iteration number; γ is the gain coefficient; δJ is the variation of system performance metric J, which is the judgment value; δU are small random perturbations having identical amplitudes and a Bernoulli probability distribution; i and j are two pixel index numbers in the evaluated local area image; p_i and p_j are the grayscale values of the two pixels. The value J increases as the fringe pattern becomes more and more distinctive, which is clearly demonstrated for a one-dimensional case in Fig. 5. During the SPGD search, the actuators are updated until the system performance metric J reaches a preset threshold value, which depends on specific hardware and system settings. Once the threshold value (e.g., J larger than 3.0×10^5) is met, all the actuators are fixed at the current position and the second fringe relaxation step begins.

Since the SPGD method is a model-free optimization technique [8] the target null shape is not limited to a specific mode or aberration (e.g., astigmatism). Another fringe restoration example using the SPGD approach is presented in Fig. 6 along with its J value trajectory. The J value in Eq. (6) was
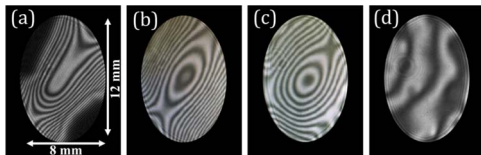
Fig. 4. Interference fringes for an in-process unknown freeform mirror (with an elliptical clear aperture) between the three SPGD searching steps. (a) The initial fringe before the searching process; (b) and (c) fringes after the first and second steps, respectively; and (d) the final interference fringe.
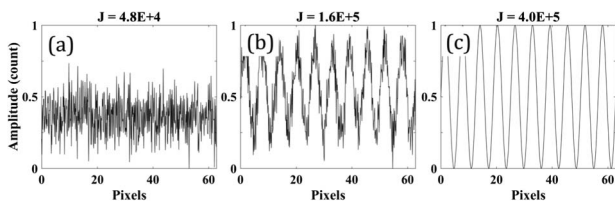
Fig. 5. One-dimensional demonstration showing the judgment value J as the fringe restoration criterion during the SPGD search process. (a) Represents the no-fringe case, (b) the middle of the restoration process, and (c) the final fringe with its J value.
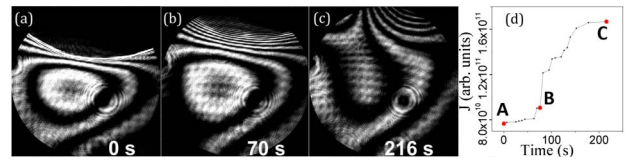
Fig. 6. SPGD-guided fringe restoration process using Eqs. (4)–(6) along with the judgment value J evolution. The full Media is given in Visualization 1 (note: $\gamma = 4 \times 10^{-10}$, J threshold = 1.67×10^{11}).

continuously evaluated while random parallel perturbations in the actuator control vector U were applied. The U vector was then iteratively updated according to Eq. (4) until the restoration process was completed.

As shown in Fig. 4(b), the no-fringe areas have been successfully recovered after the first step. However, the fringe at this step may still suffer from highly dense fringes, which means the entire metrology system is largely deviated from the null condition. The interferometric data will be adversely influenced by high-order effects, such as retrace errors [10], because the two paths (before and after reflection off the test mirror) are not the same. During the second step, the same SPGD search algorithm and DM surface updating is applied, except the judgment criterion J is simply replaced with the overall surface PV from the interferometer, and the plus sign is replaced by a minus sign in Eq. (4). Although the PV is affected by the high-order errors mentioned earlier, it is still sufficient to guide the SPGD process until it reaches the initial status for the third step, as shown in Fig. 4(c). In our experiment, the second step J value threshold was set to 4 µm PV. [Note: Other statistical values such as the root mean square (RMS) can also be used as a threshold criterion according to a specific system or need].

The third step is a global optimization process, during which the entire area of the test surface is monitored and all actuators are simultaneously updated. Instead of blindly initiating the third SPGD process, the initial surface map for the third step [e.g., Fig. 4(c)] is decomposed to Zernike modes, and the DM is updated to compensate for the same amount of wavefront deformations. After the first deterministic update, the same SPGD approach used in the second step is applied with a more rigorous J value threshold. In our study, the J value threshold in the third step was set as <500 nm PV. After the three steps, near-null interference fringes [Fig. 4(d)] are obtained, and an accurate test surface map can be calculated.

An interferometric adaptive null testing system was built as shown in Fig. 7. A Zygo interferometer (4″ Verifire ATZ) was used with a standard transmission flat. A liquid crystal display
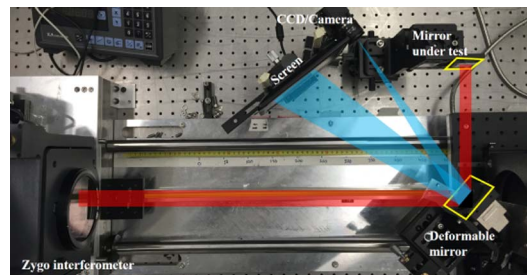
Fig. 7. Interferometric adaptive null testing system using a Zygo interferometer. Red area indicates the beam path of the interferometer, while the blue area indicates the DS beam path.

(Mimo Inc., UM-710S, 7″, 800 × 480 pixels) and a charge-coupled device (CCD) camera (PointGrey Inc., Flea3 1.3 MP Mono USB3 Vision, VITA 1300) were configured for the DS subsystem. For the adaptive null component, a membrane DM (ALPAO Inc., DM52-25, 15 mm pupil diameter, 52 actuators, 15 μm 3 × 3 stroke range) was used.

The mechanically pinched/distorted mirror with an elliptical (12 mm × 8 mm) aperture was tested in the metrology system. As mentioned earlier, the mirror was not measurable, as shown in Fig. 8(a), due to its incomplete interference fringes shown in Fig. 4(a). The adaptable null, DM, was driven through the three SPGD-based steps to realize a near-null condition shown in Fig. 4(d).

The interferometer's raw measurement ΔS_n is acquired from the final fringes with 390.44 nm PV and 46.83 nm RMS as presented in Fig. 8(b). The final optical null S_n of the DM surface was measured as 15.40 μm PV and 2.85 μm RMS [Fig. 8(c)]. Finally, we obtained the unknown mirror surface shape S_t with 15.79 μm PV and 2.89 μm RMS in Fig. 8(d) after processing the interferometer data ΔS_n and S_n together by considering the ray-path in the final null configuration [11].

We note that there are always some additional difficulties and uncertainties combined with imperfect modeling of the entire metrology system, such as unknown hardware noise and mapping between multiple maps in the data-processing pipeline. As the test optic reaches its ideal shape in the manufacturing process, however, the DM will eventually converge to a flat (or a modeled nominal shape), and the high-order effects and uncertainties will be greatly reduced. Also, although the SPGD method's convergence rate depends on many factors, such as the number of DM actuators, image resolution, and computer specification, a typical search time for the presented case studies was about 6–9 min.

To confirm the fidelity of the presented technique, a mirror, which was also measurable by the Zygo interferometer, was measured using the adaptive interferometric null testing system, as presented in Fig. 9. (Note that the mirror in Fig. 8 could not be cross-checked because it was not measurable by the interferometer.) The adaptive null technique measured the mirror shape with 1.810 μm PV and 0.365 μm RMS, as shown in Fig. 9(a). The Zygo data in Fig. 9(b) show 1.822 μm PV and 0.370 μm RMS. The direct difference map is also presented in Fig. 9(c) with 101.36 nm PV and 18.07 nm RMS.

The critical limit of the presented method is set by the available DM, which is used as an updatable null component, because this metrology concept leverages readily available adaptive optics technology. In our study, an unknown freeform optic with 12 mm × 8 mm clear apertures and ~15 μm PV was successfully measured using the specific ALPAO DM model.
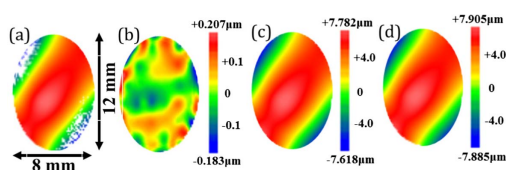
Fig. 8. (a) The unknown mirror surface with a large astigmatic error was not measurable using interferometer. (b) Raw data from the interferometer after adaptive nulling. (c) The *in situ* optical null surface shape S_n from DS. (d) Fully processed final surface map of the unknown mirror.
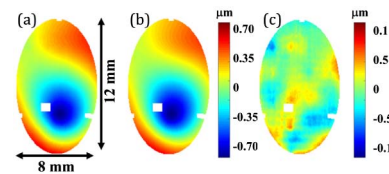
Fig. 9. Known mirror was measured to cross-confirm the measurement results. (a) The result using the adaptive interferometric null testing method. (b) The mirror shape measured by the Zygo interferometer. (c) Shows the direct subtraction between (a) and (b). The four rectangular masks are from fiducial markers to assist the mapping process.

In consideration of recent DM-related studies and developments [12–14], we expect that in-process unknown freeform optics with stronger departure values (e.g., 35 μm) can be measured.

We report an adaptive interferometric null testing method to overcome the dynamic range limitations of conventional null testing approaches, and this method is especially useful for guiding computer-controlled optics-manufacturing processes, which require the measurement of not-yet-ideal surfaces. A deformable mirror acts as an adaptable null component, and its shape is controlled by the SPGD-based search algorithm with an *in situ* deflectometry measurement system. The adaptive metrology system was designed and built using a Zygo interferometer. The experimental results successfully demonstrated its capability in measuring an unknown optical surface, which was cross-confirmed by independent interferometer-only data.

REFERENCES

1. R. A. Jones, Photon. Spectra **17**, 34 (1963).
2. D. W. Kim, S. W. Kim, and J. H. Burge, Opt. Express **17**, 21850 (2009).
3. J. C. Wyant and V. P. Bennett, Appl. Opt. **11**, 2833 (1972).
4. P. Zhou and J. H. Burge, Appl. Opt. **46**, 657 (2007).
5. H. M. Martin, J. H. Burge, J. M. Davis, D. W. Kim, J. S. Kingsley, K. Law, A. Loeff, R. D. Lutz, C. Merrill, P. A. Strittmatter, M. T. Tuell, and S. N. Weinberger, and S. C. West, Proc. SPIE **9912**, 99120V (2016).
6. T. Su, S. Wang, R. E. Parks, P. Su, and J. H. Burge, Appl. Opt. **52**, 7117 (2013).
7. P. Su, R. E. Parks, L. Wang, R. P. Angel, and J. H. Burge, Appl. Opt. **49**, 4404 (2010).
8. M. A. Vorontsov and V. P. Sivokon, J. Opt. Soc. Am. A **15**, 2745 (1998).
9. R. Huang, P. Su, J. H. Burge, L. Huang, and M. Idir, Opt. Eng. **54**, 084103 (2015).
10. W. Cai, D. W. Kim, P. Zhou, R. E. Parks, and J. H. Burge, in *International Optical Design Conference and Optical Fabrication and Testing*, OSA Technical Digest (CD) (Optical Society of America, 2010), paper OMA7.
11. J. H. Burge, W. Davison, H. M. Martin, and C. Zhao, Proc. SPIE **7018**, 701814 (2008).
12. R. Toda and E. H. Yang, J. Micromech. Microeng. **17**, 1715 (2007).
13. L. Huang, X. Ma, M. Gong, and Q. Bian, Opt. Express **23**, 17520 (2015).
14. P. Rausch, S. Verpoort, and U. Wittrock, Proc. SPIE **8447**, 844764 (2012).